processes

MDPI

Article

Study on Improvement of Acidizing Fracturing Formula in Carbonate Reservoir

Leyan Shi and Fengpeng Lai *

School of Energy Resources, China University of Geosciences (Beijing), Beijing 100083, China; leyanshi2005@163.com
* Correspondence: laifengpeng@cugb.edu.cn; Tel.: +86-010-82322005

Abstract

Addressing the challenges of poorly developed fractures and low individual well water yields within the Tianjin Ordovician–Wumishan carbonate thermal reservoir, alongside the rapid reaction rates and short effective distances observed during conventional acid fracturing operations, this study employed an XRD core analysis to confirm reservoir calcite contents exceeding 90%. Based on this finding, an acid formulation incorporating a 2% SPR-12 retarder was developed. High-temperature high-pressure reactor experiments demonstrated that this system successfully reduced the acid–rock reaction rate from 0.122 $g\cdot min^{-1}\cdot cm^{-2}$ to 0.037 $g\cdot min^{-1}\cdot cm^{-2}$ and increased the retardation efficiency from 34.07% to 68%. This significantly extended the acid penetration distance and enhanced the fracture network connectivity within the reservoir. The field trial conditions informed the parameter optimization via E-StimPlan® 3D simulations, ultimately determining that a fracture extension of 400 m could be achieved with a 20 MPa breakdown pressure. Conductivity experiments validated that a flow rate of 1.3 m^3/min generated pillar-supported wormhole structures, yielding a final conductivity of 46.8 $\mu m^2\cdot cm$. The pumping pressure plummeted from 20 MPa to 1 MPa, confirming effective fracture network communication. Gas lift backflow for 20 h mitigated secondary precipitation risks. After implementation, the water production rate of this well increased from 12.33 m^3/h to 95 m^3/h, with a dynamic water level of 158.85 m. The water temperature rose from 62 °C to 88 °C and remained stable. Compared to current acidizing and fracturing methods applied in geothermal wells, the new acid fluid system and process have increased the geothermal production capacity by 275.8%, while reducing acid consumption by 50%, providing critical technological support for the efficient development of carbonate thermal reservoirs.

Keywords: acid fracturing; geothermal wells; retarder; three-dimensional simulation

Check for updates

Academic Editor: Minghui Li

Received: 8 December 2025
Revised: 16 January 2026
Accepted: 3 February 2026
Published: 5 February 2026

1. Introduction

The Tianjin region in China is rich in geothermal resources. The area where these resources are found accounts for 81% of the city's total area, making it the largest city in China for geothermal development and utilization, with the most diverse modes of use. Geothermal energy is widely used in Tianjin for applications such as residential heating, thermal power generation, hot spring health care, and agricultural planting and breeding, which are crucial to the national economy and people's livelihood. Currently, six thermal reservoirs have been discovered (Figure 1a), which are influenced by four geological fault zones [1,2]. These reservoirs are distributed in three dimensions within a depth range of 300–4000 m (Figure 1b), with suitable temperatures ranging from

25 °C to 103 °C; the highest water temperature recorded in geothermal wells is 113 °C. The water yield per well ranges from 40 to 120 m^3/h, and the water quality meets satisfactory standards for utilization [3–5]. After evaluation, the total exploitable amount of geothermal fluid in all thermal reservoirs in the city amounts to 496 million cubic meters per year. The annual available amount is 17.48 billion gigajoules. It is predicted that by 2025, the area of geothermal heating alone will reach 60 million square meters.

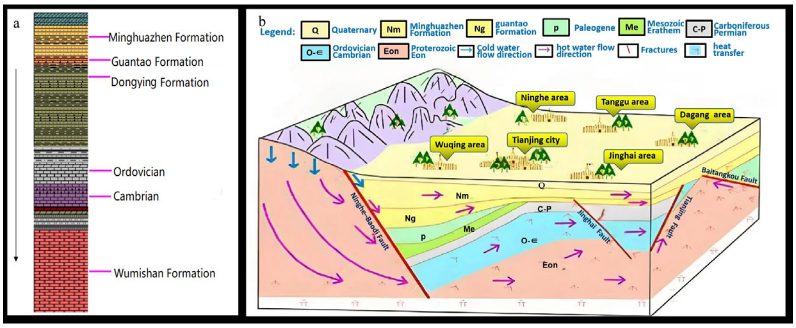

Figure 1. (**a**) Comprehensive Core Column Diagram of Tianjin Area, (**b**) Geological structure map of geothermal resources in Tianjin area.

The Ordovician carbonate rocks and Wumishan Formation dolomite of the Jixian Series are the main target layers for geothermal resource development due to their diverse reservoir space types, large reservoir thickness, wide regional distribution, and good continuity [6,7]. However, in actual development processes, a key technical bottleneck is commonly encountered: insufficient water output from individual wells [8–10] (Table 1). The causes of this issue are complex and varied, mainly including low reservoir permeability; significant heterogeneity in the thermal reservoir, with an insufficient development of local seepage channels; and the poor connectivity of the natural fracture network in some areas of the thermal reservoir. Insufficient production capacities of individual wells directly restrict the overall development scale and economic benefits of geothermal reservoirs, making it urgent to adopt effective reservoir modification measures to increase production [11–13].

Table 1. The utilization rates of various geothermal reservoirs in Tianjin.

Thermal Reservoir		Thermal Efficiency
Newly Related Pore Type	The Minghuazhen Formation	18.04%
	Guantao Formations	44.44%
Basement karst fissure type	Ordovician Formation	27.93%
	Changwu Formation	48.52%
	Wumishan Formation	63.66%

To break through production capacity bottlenecks and improve the efficiency of geothermal resource development, researchers have adopted acid fracturing enhancement technology from oil and gas reservoir development experience, achieving significant results. The core of this technology lies in the following process: using high-pressure surface pumping equipment (Sichuan Bomco Special Vehicle Manufacturing Co., Ltd, Deyang, Sichuan province, China) to inject a specialized acid system into the target geothermal reservoir interval at high speed. Under sufficiently high injection rates, the downhole pressure quickly exceeds the breakdown pressure of the reservoir rock, creating new fractures or opening existing natural fractures. Simultaneously, the acid flows along the fracture walls, undergoing chemical dissolution reactions with the fracture surfaces. This significantly widens the fractures and etches uneven grooves on the walls, enabling the fractures to maintain high conductivity even under closure stress [14,15]. This process effectively expands the fracture network, improves the reservoir's flow channels, and substantially increases the output capacity of geothermal fluids. As early as the beginning of this century, domestic and international scholars began exploring and reporting the application of acid fracturing technology in geothermal reservoir transformation [16–20]. With the accumulation of practical experience and deeper research, a series of key models and mechanisms—such as acid–rock reaction dynamics, fracture extension simulations, acid loss control, and conductivity prediction—have been extensively proposed and refined to address the characteristics of geothermal reservoirs [21–23]. For example, Lin Tianyi et al. conducted systematic research on the mechanisms of acid fracturing enhancement for geothermal reservoirs in the Beigong'an area of Beijing [24–26]. Through physical simulation experiments and site data analysis, they confirmed that the effectiveness of acid fracturing is closely related to the geological characteristics of the reservoir, and the more developed the natural fractures and joints (structural weak planes) in the reservoir, the more effectively the acid can communicate and form complex and effective fracture networks. Additionally, the higher the content of carbonate rocks in the reservoir, the higher the efficiency of acid dissolution, leading to a stronger conductivity of the resulting dissolution fractures and better enhancement effects [27–29]. This understanding provides important geological criteria for selecting suitable target zones for acid fracturing.

To address the widespread issue of insufficient water production in the carbonate rock geothermal reservoirs of the Ordovician and Jixian systems in the Mengxianshan Formation in Tianjin, it is imperative to conduct in-depth research on the application foundation and optimization of acid fracturing technology under these specific geological conditions to effectively enhance the productivity of geothermal wells. This study will focus on the following aspects: (1) systematically analyzing the composition of carbonate rocks in the geothermal reservoirs of Tianjin; (2) developing and screening efficient and slow-release acid systems, with a particular emphasis on solving high-temperature, slow-release, and deep penetration issues, while investigating the acid–rock reaction behavior under varying temperatures and pressures; and (3) evaluating and optimizing acid fracturing process models suitable for the local geological and mechanical conditions and reservoir properties (such as temperature and permeability characteristics), as well as optimizing operational parameters. Through these systematic studies, this research aims to provide a solid theoretical foundation and technical support for acid fracturing operations to enhance geothermal reservoir productivity in Tianjin and similar carbonate rock geothermal reservoirs in North China, contributing to the large-scale development of local geothermal resources.

2. Results and Discussion

2.1. Improvement of Acidizing Fluid Formulation

The biggest difference between the construction process of geothermal wells and oil and gas wells lies in cost control. Since the revenue from geothermal wells is far less than that from oil and gas wells, it is essential to strictly control costs in the construction of geothermal wells. Therefore, the construction techniques for oil and gas wells cannot be fully adopted, and this also applies to acid fracturing. To control costs, some geothermal well acidizing fluids only use hydrochloric acid or add a small amount of corrosion inhibitors and iron ion stabilizers. This formulation has a certain effect on some formations with well-developed fractures, but the effect is not significant in formations with poorly developed fractures. The fracturing pressure of geothermal wells is generally 10–20 MPa, which causes damage to the surrounding rocks of the wellbore. The more significant matter is to drive the acidizing fluid through the fractures to react with rocks that are further away from the wellbore, thereby expanding the fractures. Since hydrochloric acid is strong and reacts quickly with carbonate rocks—especially in high-temperature geothermal wells, where the reaction speeds are even faster—the acidizing process is almost finished before reaching the predetermined fracturing distance. This results in a limited treatment range, leading to acidizing fracturing only working to expand the fractures around the wellbore and failing to establish communication with distant fractures. This has resulted in the improvement effects on the fractures not being obvious. Therefore, many geothermal wells require multiple acidizing fracturing operations to achieve desired results [30,31].

Carbonate rocks are primarily composed of calcite and dolomite minerals. Hydrochloric acid (HCl) is commonly used as a solution to react with carbonate rocks, generating water-soluble $CaCl_2$ and $MgCl_2$, which assist with fracture opening [32]. The chemical equations for the acidizing reactions are as follows:

$$2HCl + CaCO_3 = CaCl_2 + H_2O + CO_2\uparrow \tag{1}$$

$$4HCl + CaMg(CO_3)_2 = CaCl_2 + MgCl_2 + 2CO_2\uparrow + 2H_2O \tag{2}$$

The conventional acidizing fluid formula for carbonate geothermal wells typically contains hydrochloric acid at a certain concentration, supplemented by corrosion inhibitors, iron ion stabilizers, defoamers, and clean water. To solve this problem in current practical application processes, most acid systems rely on viscosity to reduce the acid–rock reaction rate, thereby effectively extending the live acid penetration distance. This is particularly true for gelled acid systems. During treatment operations, the inherent viscosity of these systems creates high frictional pressure losses within the pumping lines, resulting in reduced field injection rates. Simultaneously, the gelling agent molecules are susceptible to degradation under downhole conditions (pressure and temperature), undergoing coil contraction or breakage. This leads to a decline in fluid viscosity, accelerating hydrogen ion mobility and consequently increasing the acid–rock reaction rate, shortening the effective live acid distance. Other retarded acid systems, such as emulsified acids and foamed acids, often suffer from difficulties during pumping or cause significant formation damage. Furthermore, an excessive residual acid discharge poses serious environmental pollution challenges.

The acid spending rate is influenced by multiple factors, including the H^+ generation rate, the mass transfer rate of H^+ to the rock surface, and the removal rate of reaction products from the mineral surface [33]. Reducing frictional losses and optimizing viscosity enhances pump efficiency and improves the effective transport distance of live acid within the formation. Therefore, achieving effective reservoir etching by acidizing fluids hinges on controlling the reaction kinetics between the acid and the rock matrix. Based on this reaction mechanism, this study developed SPR-12 (Shengli Oilfield Fangyuan Chemical Co., Ltd., Dongying, Shandong, China), a retarder formulated through a synergistic combination of nitrogen-containing heterocyclic compounds and cationic surfactants. Optimal corrosion inhibitors, ferric ion stabilizers, and flowback aids were also selected. The optimized retarded acid system for this study was formulated as follows: 20% HCl supplemented with a 2% SPR-12 retarder, a 3% corrosion inhibitor, a 1.5% iron stabilizer, and a 1% displacement aid (Figure 2). This specific composition was developed to ensure effective deep-penetration etching while maintaining system stability and wellbore integrity under high-temperature reservoir conditions. The optimized retarded acid system for this study was formulated as follows: 20% HCl supplemented with a 2% SPR-12 retarder, a 3% corrosion inhibitor, a 1.5% iron stabilizer, and a 1% displacement aid (Figure 2). This specific composition was developed to ensure effective deep-penetration etching while maintaining system stability and wellbore integrity under high-temperature reservoir conditions.

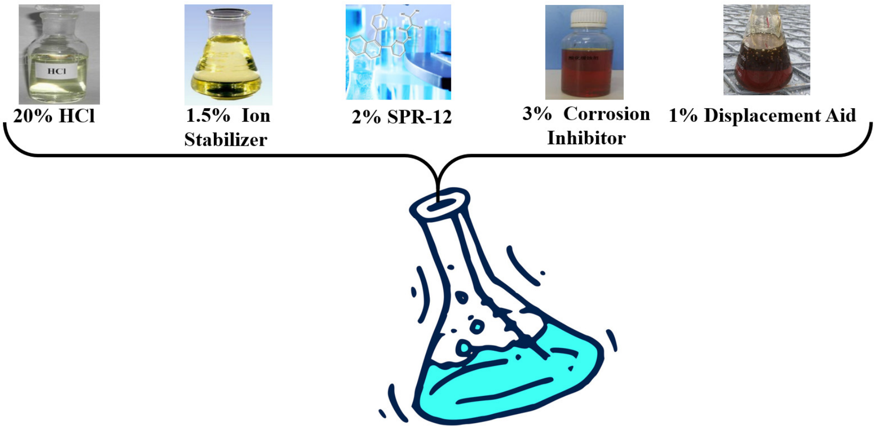

Figure 2. The new acidizing solution formula.

2.2. Performance of the New Retarded Acid System

2.2.1. Static Acid–Rock Reaction Rate

Core samples from development wells are used in this study, as shown in Figure 3. By adopting high-temperature and high-pressure acid–rock reaction vessel experiments, based on the water temperature reference from adjacent wells and reasonable assumptions for a modified water temperature of 85 °C, we tested the dissolution rate, dissolution velocity, and retardation ratio relative to the 20% hydrochloric acid setup of common retarded acid systems and novel retarded acid systems at 85 °C. The experimental results are presented in Table 2.

Figure 3. Five types of core appearance.

Table 2. Retarding Effects of Different Acid Systems.

Acid System	Dissolution Rate (%)	Dissolution Rate (g/min)	Retardation Efficiency (%)
20% HCl	55.94	0.7648	—
Polyhydroxon Acid	38.72	0.3897	30.78
Gelatinized Acid	36.88	0.3289	34.07
Emulsified Acid	38.34	0.3721	31.46
Foamed Acid	37.29	0.3624	33.34
New Retarded Acid System	17.51	0.2168	68.69

Under 85 °C conditions, the maximum retardation efficiency of other retarded acid systems relative to 20% HCl was 34.07%, while The New Retarded Acid System achieved a significantly higher value of 68.69%, demonstrating a superior retardation performance.

2.2.2. Core Retardation Experiment

Core samples from development wells were collected in order to conduct experiments with conventional acid fluids and a New Retarded Acid fluid containing a retarder.

After conducting five experiments and adjusting the standard deviation, the average data obtained are shown in Table 3. Relative to a blank acid fluid without a retarder, The New Retarded Acid System containing SPR-12 exhibits a significantly reduced acid–rock reaction rate, stabilizing at approximately 0.037 $G \cdot min^{-1} \cdot cm^{-2}$. The calculated retardation rate exceeds 68%.

Table 3. Acid–Rock Reaction Rates.

Core Lithology & Acid System	Acid–Rock Reaction Rate ($G \cdot min^{-1} \cdot cm^{-2}$)	Retardation Rate (%)
Bed 26 (Conventional Acid)	0.122425	0
Bed 26 (New Retarded Acid)	0.03782	69.11
Bed 27 (New Retarded Acid)	0.03679	69.95
Bed 28 (New Retarded Acid)	0.03768	69.23
Bed 29 (New Retarded Acid)	0.03864	68.44
Bed 30 (New Retarded Acid)	0.03867	68.42

2.2.3. Retarding Performance at Different Temperatures

The temperature resistance of The New Retarded Acid System was assessed by measuring its retardation efficiency relative to 20% HCl across varying temperatures.

Figure 4 indicates that the retardation efficiency gradually decreased with increasing temperatures. Below 140 °C, the decline was minimal; however, above 160 °C, a sharp reduction occurred. This indicates a significant degradation of The New Retarded Acid System above 160 °C, confirming its operational temperature limit of up to 140 °C.

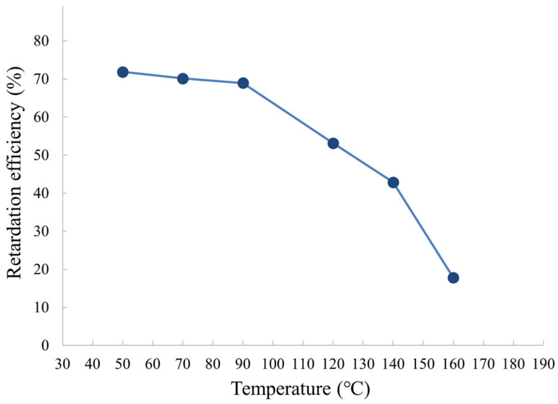

Figure 4. Retardation Efficiency of The New Retarded Acid System at Different Temperatures.

2.2.4. Rock Alteration Effects of Retarded Acid Systems

Conductivity experiments compared the post-acidizing flow capacity of carbonate reservoir rocks treated with 20% HCl versus The New Retarded Acid System, evaluating reservoir stimulation efficacy. The results are summarized in Table 4. Under identical pressure differentials and flow rates, The New Retarded Acid System achieved a conductivity of 318.31 D·cm, outperforming the conventional HCl system.

Table 4. Conductivity Test Results.

System	Flow Rate (mL/min)	Viscosity (mPa·s)	Conductivity (D·cm)
20% HCl	5	0.9	255
New Retarded Acid System	5	0.9	318

The enhanced performance is attributed to localized corrosion near the acid entry point in HCl-treated samples, where rapid reactions depleted the H^+ concentration toward the core outlet. In contrast, The New Retarded Acid System formed a molecular adsorption layer during corrosion, mitigating further acid penetration and sustaining high H^+ concentrations deeper into the core for uniform wormholing.

2.2.5. Mechanism Study

The New Retarded Acid System employs nitrogenous heterocyclic compounds and cationic surfactants that rapidly wet and adsorb onto rock surfaces via electrostatic attraction and hydrogen bonding, forming monolayer/multilayer barriers. These structures (Figure 5) reduce reaction kinetics by limiting H^+–rock surface collisions, lowering interfacial tension to minimize capillary trapping within pores, and enhancing acid propagation through the formation matrix. This synergistic mechanism optimizes deep diversion while maintaining controlled reactivity.

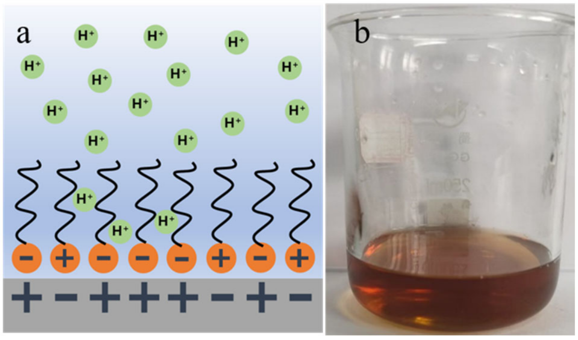

Figure 5. (**a**) Retarded agent adsorption film-forming mechanism diagram, (**b**) Appearance of the acid solution.

2.3. Optimization of Acid Fracturing Process

The optimization of acid fracturing operations in carbonate reservoirs primarily focuses on pumping sequences and alternating injection stages, while also considering the subsequent flowback timing and methodology.

Firstly, the primary function of the preflush fluid is to initiate fracture creation and reduce the near-wellbore fracture temperature. An optimized approach utilizes a NH_4Cl solution injected into the formation. This liquid acts to precondition the reservoir, establishing an initial fracture network. The solution leverages its heat capacity to absorb geothermal energy, effectively lowering the temperature within the near-wellbore region. Ensuring the complete filling of the annulus below the packer with the preflush fluid creates a stable environment for subsequent acid injections.

Secondly, a dynamic injection strategy involving alternating stages of acid and displacement fluid is employed. During this process, the acid reacts with the carbonate rock surface. Non-uniform etching along the fracture walls generates highly conductive flow channels. Under sustained pressure, the initial fracture propagates and branches, ultimately forming a complex fracture network. The displacement fluid serves to displace residual acid from the wellbore and near-fracture zones, driving the active acid deeper into the fracture system. This significantly extends the effective treatment penetration depth. This alternating injection sequence mitigates premature acid depletion, enabling deep penetration and enhanced etching efficiency.

Finally, during the flowback control phase, high-concentration HCl reactions generate substantial volumes of CO_2 and secondary precipitates. Any retained fluid within the formation poses a severe risk of blocking the newly created flow pathways. CO_2 exists in a supercritical state under reservoir conditions, exhibiting properties of both gaseous low viscosity and a liquid-like high density, conferring strong solvent power. Conventional blowdown methods are ineffective for its removal. Therefore, a combined flowback procedure is mandatory. Following an initial blowdown to remove a portion of fluids, immediate gas lifting operations must commence. The gas lift mandrel depth must be sufficient to disrupt the supercritical CO_2 state [34] (reducing bottomhole pressure below 7.38 MPa). Sustained pressure reduction facilitates the transition of CO_2 to a gaseous state for efficient expulsion. Minimizing the residence time of the residual acid is critical to prevent renewed solid precipitation. Field experience confirms that flowback efficiency directly impacts the sustainability of fracture conductivity and is paramount for ensuring the effectiveness of acid fracturing treatments (Figure 6).

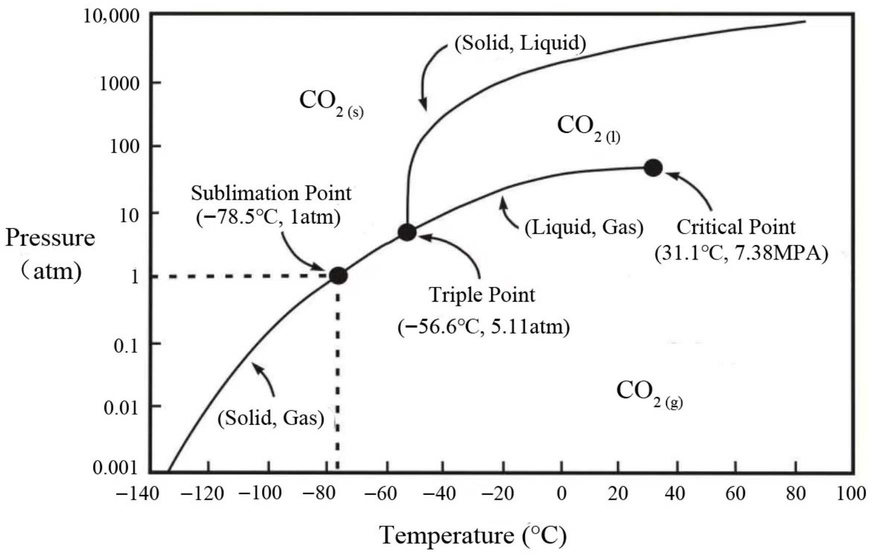

Figure 6. Phase diagram of CO_2 physical properties.

The timeliness of the flowback can significantly impact the effectiveness of acid fracturing, yet it is often overlooked by technical staff. In a nearby geothermal well with a similar casing structure, geological conditions, acid fracturing formulation, and construction processes, the acid fracturing effect was suboptimal due to a 2-day delay in gas lift venting caused by weather conditions, resulting in minimal production enhancements.

2.4. Experimental Simulation of Acid Etching and Flow Conductivity Capability of the New Retarded Acid System

The New Retarded Acid System and core samples were employed to evaluate the etching morphology of acid-etched fractures and their flow conductivity capabilities. The experimental results and descriptions of erosion patterns are presented in Table 5, while post-acidizing core sample photographs are shown in Figure 7.

Table 5. The New Retarded Acid System etching morphology results.

Core Type	Initial Fracture Width/mm	Acid Injection Volume/mL	Flow Rate/mL/min	Experimental Temperature/°C	Erosion Morphology Description
26	2	6000	1000	85	Erosion is relatively uniform. Grooves are shallow
26	2	6000	1100	85	Erosion is relatively uniform with certain roughness
26	2	6000	1200	85	Arch-type support, Grooves are deep, with wormholes
26	2	6000	1300	85	Pointed support, Grooves are shallow
27	2	6000	1300	85	Arch-type support, Grooves are obvious, with wormholes
28	2	6000	1300	85	Pointed support, Grooves are shallow
29	2	6000	1300	85	Pointed support, Grooves are shallow
30	2	6000	1300	85	Arch-type support, Grooves are deep

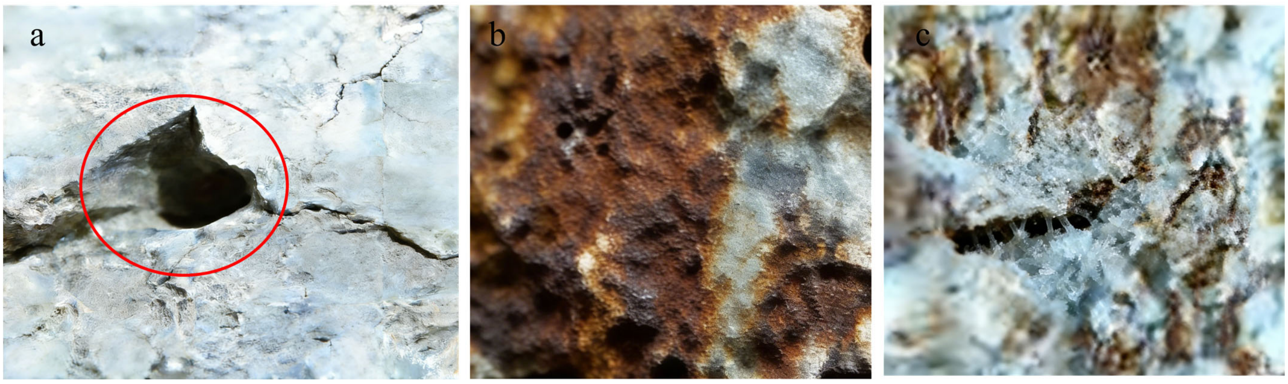

Figure 7. Rock acid erosion morphology; (**a**) wormhole state of rock plate after acid erosion; (**b**) point-like support; (**c**) bridge-pier type support.

The results of the fracture erosion characterization indicated that the core samples developed typical wormhole structures after acid erosion. The morphological features were primarily characterized by discrete spot-like pits and residual mineral pillars in a bridge-like structure. Flow capacity test data further revealed a significant positive correlation between the injection rate and fracture flow performance (Table 6). Specifically, increasing the injection rate enhances the uneven erosion of the fracture walls by the acid, thereby expanding the effective flow channels. Therefore, in engineering practice, high-rate operations should be prioritized to maximize the acid erosion flow capacity. Notably, the fracture flow capacity is highly sensitive to closure pressure: as the closure pressure increases, the supporting structures undergo plastic deformation or even failure, leading to a sharp decline in flow capacity. This highlights the critical role of reservoir stress management in maintaining production enhancement effects.

Table 6. Impact of Injection Rate on Conductivity of Acid-Etched Fractures ($\mu m^2 \cdot cm$).

Injection Rate (mL/min)	Closure Pressure (MPa)						
	0	**5**	**10**	**20**	**30**	**40**	**50**
1000	38.8	27.2	18.7	18.2	9.6	9.4	8.1
1100	49.8	39.4	27.6	18.1	13.7	11.1	9.1
1200	45	36.3	26.3	18.8	15.4	12.3	10.5
1300	46.8	37.2	27.8	19.3	15.3	12.6	10.6

2.5. Simulate Acid Fracturing Effects by the E-StimPlan

To select the optimal acid fracturing pressure and achieve the best acid fracturing effect, this paper used E-StimPlan (StimPlan Version 5.5, https://www.nsitech.com/stimplan-software/, accessed on 7 December 2025) software to simulate the acid fracturing process. E-StimPlan is a full three-dimensional fracturing design and analysis software that includes all functions for fracturing design, fracturing analysis, and optimization. It also includes the functions of acid fracturing design and fracturing filling design, which are not only suitable for conventional sandstone reservoirs but also for unconventional reservoirs. It is suitable for vertical wells, horizontal wells, and directional wells.

E-StimPlan includes the simulation of 'acidic fracturing'. The use of E-StimPlan for this simulation was intended to utilize the numerical multiphase fluid flow algorithm. Compared to the 'average' characteristics obtained from simple model calculations, it can perform detailed calculations of the acid erosion effects and flow capacity.

With the concentration of the hydrochloric acid solution determined to be 20%, the fracture parameters of the dolomite in the Wumishan Formation of the target layer (Table 7)

https://doi.org/10.3390/pr14030563

were selected and substituted into E-StimPlan for acid fracturing simulations. Multiple simulation experiments were conducted at pressures of 10 MPa, 20 MPa, 30 MPa, 40 MPa, and 50 MPa, respectively, with the average values calculated and adjusted for standard deviations. The development of the fractures is presented in a cloud map in Figure 8. Under external pressure conditions of 10 MPa, 20 MPa, 30 MPa, and 50 MPa, the fractures extended to 300 m, 400 m, 500 m, and 600 m, respectively.

Table 7. Simulated parameters.

Fracture Initiation Depth (m)	Fracture Termination Depth (m)	Thickness (m)	Porosity (%)	Compressive Strength (MPa)	Reaction Rate Constant $\times 10^6$	Reaction Activation Energy	Reaction Order
3545.5	3548.7	3.2	4.02	160			
3600.1	3608.4	8.3	3.13	160			
3627.5	3632.4	4.9	3.81	160	0.5	5000	0.5
3637.8	3641.9	4.1	4.56	160			
3648.4	3661.8	13.4	6.29	160			

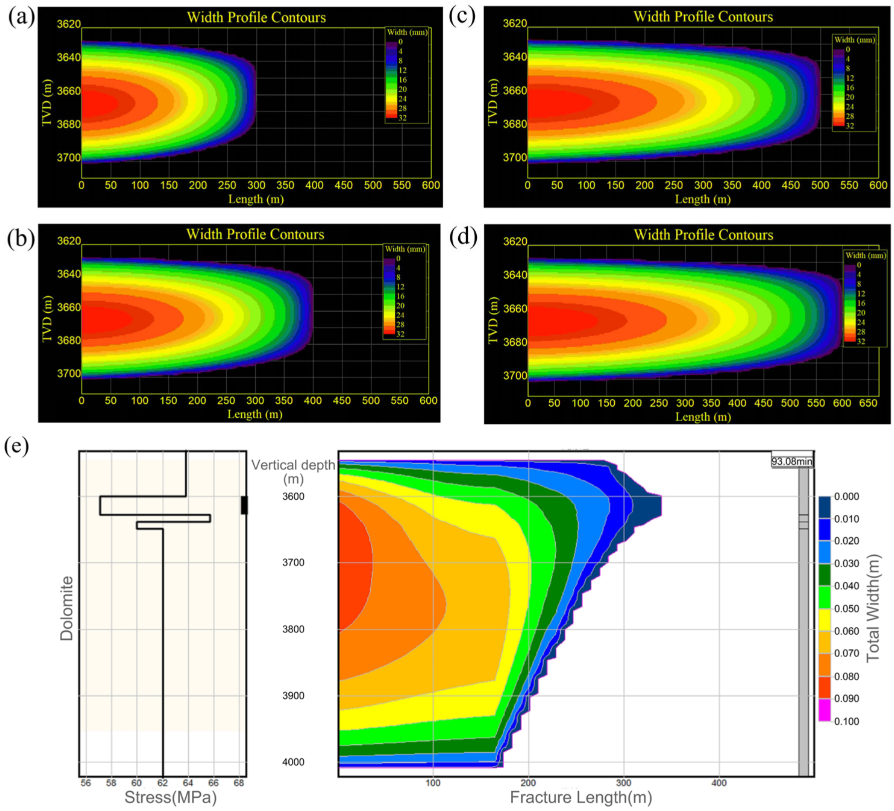

Figure 8. Simulation diagram of hydraulic fracturing pressure fracture development (**a**): 10 MPa, (**b**): 20 MPa, (**c**): 30 MPa, (**d**): 50 MPa, (**e**): 20 MPa fracture geometry diagram under acid fracturing pressure.

The key assumptions underlying the operation of E-StimPlan include geomechanical, fluid dynamic, fracture propagation model, and proppant behavior assumptions. During simulations, particular attention must be paid to the occurrence probability of various scenarios derived from these assumptions in real-world conditions. Multi-conditional assumption simulation analyses should be conducted to ensure the accuracy and reliability of the simulation results.

For instance, the fracture roughness uniformity impacts fluid flow regimes and mass transfer efficiency, while also governing proppant deposition and distribution patterns within the fracture network, thereby influencing the fracture conductivity. Simulation efforts should therefore center on fracture roughness, examining its multidimensional effects on conductivity through varied perspectives.

Another critical factor is the acid leakage behavior. Key determinants include formation permeability, porosity, fracture dimensions, connectivity, and acid properties (such as concentration and viscosity). Formations with high permeability exhibit a heightened propensity for acid diversion away from the target zone, compromising fracturing effectiveness. To mitigate this risk, repeated simulations across diverse acid concentrations and viscosities are recommended, coupled with optimized injection rates and pressure profiles for fracturing fluids.

2.6. Acid Fracturing On-Site Construction Process

The on-site operations utilized three 700-type pump trucks and one 300-type pump truck, performing staged alternating injections in three sequences. During pumping, the peak pressure reached 20 MPa, with an average displacement rate of 1.3 m^3/min. The pressure gradually decreased from 20 MPa to 1 MPa, indicating successful fracture connectivity and pressure release—confirming operational success. Fracture monitoring revealed a total acid–rock reaction time of 46 h, with the maximum effective acid penetration distance reaching 330 m. After pressure depletion, the packer and tubing string were retrieved, followed by the deployment of an 800 m coiled tubing string for gas lift-assisted flowback. To mitigate secondary precipitation risks, the interval between the completion of the acid fracturing and the initiation of gas lift unloading was strictly controlled within 20 h, as shown in Figure 9.

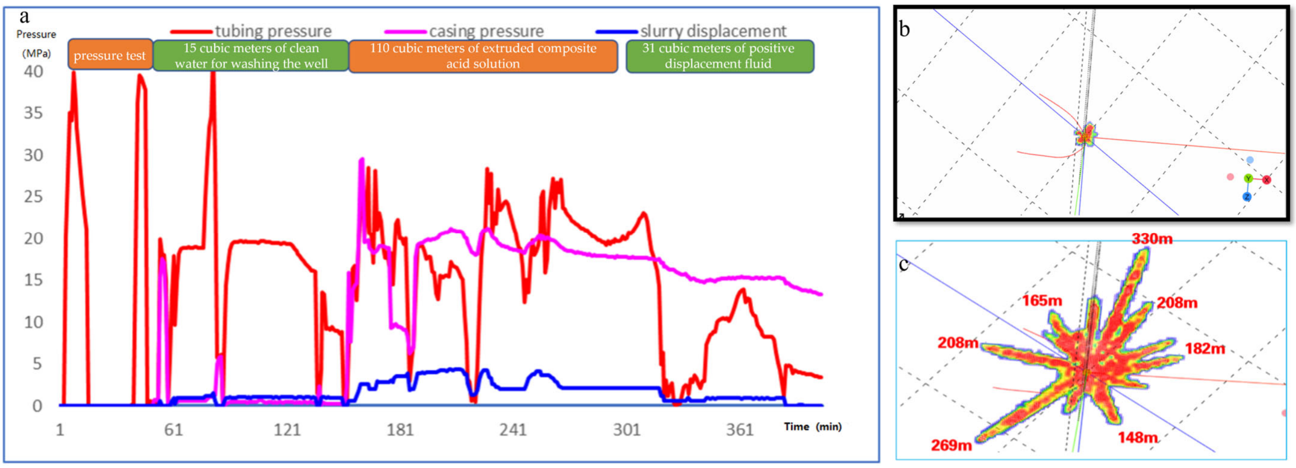

Figure 9. (**a**) Comprehensive curve of well acidization and fracturing construction, (**b**,**c**) Schematic diagram of dynamic monitoring results of fractures in an experimental well (Video S2).

2.7. Acid Fracturing Stimulation Performance

After the acid fracturing treatment, the stable water production rate of this well after reached 100.4 m^3/h, representing a significant increase compared to pre-stimulation levels. The stable dynamic liquid level was maintained at 158.85 m, while the produced fluid temperature remained constant at 90 °C. These results demonstrate that the novel acid formulation successfully activated the near-wellbore fracture network and established effective connectivity with deep flow channels. The actual fracture network extension morphology exhibits a strong consistency with the numerical simulation predictions from E-StimPlan. Compared to conventional acid fracturing schemes, The New Retarded Acid System enhanced the production efficiency while reducing the acid consumption volume, thereby showcasing its superior technical and economic advantages.

3. Conclusions

This research successfully developed and validated an efficient and cost-effective acid fracturing technology tailored for carbonate geothermal reservoirs, as demonstrated in the Tianjin region. The key outcomes are represented by several integrated aspects.

First, a novel retarded acid system was formulated using the retarder SPR-12, which contains nitrogenous heterocyclic compounds and cationic surfactants. This system achieves a retardation rate exceeding 68%, ensuring deep fluid penetration and effective fracture etching, thereby addressing the historical challenges of poor stimulation results and high acid consumption in such wells.

The geological feasibility was confirmed through a detailed core characterization, identifying the reservoir lithology as predominantly calcite, whose high solubility provides a fundamental basis for acidizing stimulation. Technologically, optimized construction techniques were established, featuring a dynamic injection mode with alternating stages of acid and displacement fluid. This design prevents premature acid depletion and facilitates deep reservoir etching. The field application in a geothermal well in Jinghai District, Tianjin, demonstrated the practical efficacy of the new system and process. The treatment resulted in a 275.8% increase in the geothermal production capacity while achieving a reduction of over 50% in hydrochloric acid consumption compared to conventional methods in similar wells, significantly enhancing production efficiency, economic viability, and clean production standards.

Furthermore, the integration of the numerical simulation (via E-StimPlan 3D) with physical conductivity experiments provided a scientific basis for optimizing key operational parameters, such as the fracture pressure and injection rate, and validated the sustained flow capacity of the created fractures.

Collectively, this work provides a comprehensive, validated technical solution and valuable practical experience for the effective stimulation of analogous carbonate geothermal reservoirs.

4. Materials and Methods

4.1. Research on Reservoir Characteristics

4.1.1. Reservoir Characteristics

The Ordovician and Jixian County Misty Mountain Group in Jinghai District, Tianjin, has been strongly influenced by the multi-stage activity of the Tianjin Fault and its secondary faults. This has resulted in a reservoir space primarily characterized by a porous–fractured–cavernous composite type. Historical production data indicate that the geothermal reservoir in this area exhibits significant production potential, as evidenced by the stable water flow rates of 127 m^3/h from the Jing 32# well and 119 m^3/h from the Jing 37# well, which demonstrate the overall good conductivity of the reservoir. However, the strong heterogeneity of the reservoir has led to an abnormal production capacity in local areas, with a maximum water flow rate of only 34 m^3/h in X# in Jinghai District, which is significantly lower than the average of other geothermal wells. This well, with a depth of 3800 m, is a four-open directional well. The target geothermal reservoir is the Jixian County Misty Mountain Group, located at a depth of 3525–3800 m, exposing 275 m of dolomite from the Misty Mountain Group. Before acid fracturing, the well had an average water production rate of 12.33 m^3/h, a dynamic water level of 250 m, and a water temperature of 62 °C. Based on log interpretation, the fracture development in the well is displayed in Table 8. There are two first- and second-class fractures with a total length of 18.3 m and three third-class fractures with a total length of 15.3 m, indicating relatively poor fracture development.

Table 8. Well logging fracture interpretation results.

Layer Number	Starting Depth (m)	Termination Depth (m)	Thickness (m)	Porosity (%)	Permeability (10^{-3} μm^2)	Mud Content (%)	Well Temperature (°C)	Explain the Conclusion
26	3545.5	3548.7	3.2	4.02	0.35	1.64	87.1	Three types of fractured layers
27	3600.1	3608.4	8.3	3.13	0.22	1.57	87	Three types of fractured layers
28	3627.5	3632.4	4.9	3.81	0.35	1.94	87.6	Two types of fractured layers
29	3637.8	3641.9	4.1	4.56	0.74	1.66	88.1	Three types of fractured layers
30	3648.4	3661.8	13.4	6.29	1.65	1.90	88.8	one type of fractured layers

4.1.2. Mineral Composition of the Reservoir

The rock core samples from layers 26 to 30 of this well were analyzed via a whole-rock mineral quantitative analysis using XRD. The results are shown in Table 9. The mass fraction of carbonate minerals in the reservoir exceeds 90%, with calcite ($CaCO_3$) being the dominant carbonate mineral and the remaining portion consisting of a small amount of dolomite [$CaMg(CO_3)_2$]. Due to the high content of calcite in the rock properties of the reservoir, the development of the acid system formulation and acidizing simulation must take into account the influence of the rock property distribution.

Table 9. Core mineral quantitative analysis table (mass concentration).

Layer Number	Mica	Quartz	Potassium Feldspar	Plagioclase	Hematite	Dolomite	Calcite	Pyrite	Total Clay Content
26		2.5%				4.5%	89.6%		3.4%
27		3.2%				1.9%	87.1%		7.8%
28		1.2%				18.5%	73.1%		7.2%
29		2.7%				14.3%	78.5%		4.5%
30		5.1%				0.5%	94.4%		/

The carbonate rock content in Jinghai, Tianjin, is classified based on the contents of calcite and dolomite. Details are as follows in Table 10.

Table 10. Tianjin Jinghai Carbonate Rock Composition.

Rock Type	Calcite Content (%)	Dolomite Content (%)	Ratio of CaO to MgO
Pure Limestone	100-95	0-5	>50.1
Limestone with Dolomite	95-75	5-25	50.1-9.1
Dolomitic Limestone	75-50	25-50	9.1-4.0
Argillaceous Dolomite	50-25	50-75	4.0-2.2
Dolomite with Limestone	25-5	75-95	2.2-1.5
Pure Dolomite	0-5	95-100	1.5-1.4

4.2. Research on Acid Liquid System

The transfer rate of H^+ controls the speed of the acid–rock reaction. As such, by changing the acidification formula, reducing the transfer rate of the H^+ and carbonate rock, the reaction speed was reduced, and the effective action distance of the acid solution was increased. Therefore, in the present study, a combination of hydrochloric acid and formic acid was initially employed for the experiment, which yielded unsatisfactory results.

Formic acid, also known as ant acid, is a weakly ionized organic acid characterized by a slow reaction, and it reacted slowly with carbonate rocks and exhibited weak corrosiveness. It also resulted in a slow-release and corrosion-inhibiting effect at higher temperatures. The chemical equation of the reaction was as follows.

$$2HCOOH + CaCO_3 = Ca(COOH)_2 + H_2O + CO_2\uparrow \quad (3)$$

$$4HCOOH + CaMg(CO_3)_2 = Ca(COOH)_2 + Mg(COOH)_2 + 2CO_2\uparrow + 2H_2O \quad (4)$$

However, the reaction between formic acid and carbonate rocks can easily lead to precipitation, which blocks the seepage channels. Therefore, high concentrations of formic acid should not be used; generally, the concentration should not exceed 10%.

The relationship between the concentration of hydrochloric acid and the reaction rate is presented in Figure 10. When the concentration of hydrochloric acid was less than 20%, the reaction rate increased with the increase in the concentration; when the concentration of hydrochloric acid exceeded 20%, this trend slowed down; when the concentration reached 22–24%, the reaction rate reached the maximum value; and when the concentration exceeded this value, the reaction rate decreased with the increase in the concentration. When concentrated acid was used as the acidizing fluid, its reaction rate was much slower than that of fresh acid at the same concentration when it became residual acid. Due to the high viscosity of the high-concentration hydrochloric acid, which helps to reduce filtration loss, the concentration of hydrochloric acid in the acidizing fluid should be maintained around 20%. The specific concentration of hydrochloric acid can be determined according to the rock debris acid dissolution test.

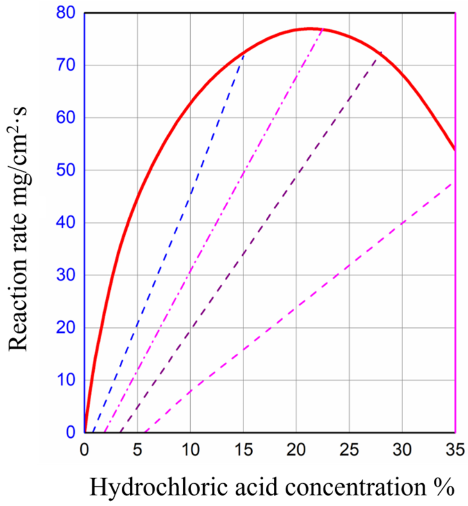

Figure 10. The curve of the relationship between the concentration of hydrochloric acid and the reaction rate.

Corrosion inhibitors and iron ion stabilizers can effectively reduce the corrosion of acid solutions on well pipes, decrease hydrogen production, and ensure construction safety. The new acidizing solution formula contained 20% hydrochloric acid and 10% formic acid. In the experiment, an acidizing fluid system composed of 20% hydrochloric acid, 10% formic acid, a corrosion inhibitor, and a ferrous ion stabilizer was employed. However, this formulation was abandoned during testing due to the instability of the acid solution and its high consumption rate.

4.3. Static Acid–Rock Reaction Experiment

The experiment was conducted using a high-temperature and high-pressure acid–rock reaction vessel, with 250 mL of acid solution added per test. The carbonate rock core measured 4.0 cm in length and 2.5 cm in diameter and was encapsulated in epoxy resin with only one end face exposed, resulting in a reactive contact area of 5.0 cm^2. The core reacted with different acid systems at 85 °C for 1 h under controlled conditions. Each test consisted of three replicates, and the pressure was incrementally increased in steps of 2 MPa. The temperature was controlled with a precision of 85 °C ± 0.5 °C. The agitation strategy employed stepwise variable speed adjustments, with a focus on identifying critical thresholds. Real-time synchronized monitoring and logging of pH, conductivity, and turbidity was performed concurrently. Prior to testing, pre-pressurization with nitrogen was conducted to verify the seal integrity of the reaction vessel.

The testing was staged and relevant data was shown in the Table 11. A baseline was first established at 5 MPa and 400 RPM, after which subsequent experiments were performed by modifying only a single variable at a time. For emergency handling, an abrupt pressure drop exceeding 0.5 MPa per minute triggered an immediate automatic system shutdown for leak inspection. During data processing, the experimental error was effectively reduced by averaging the results from multiple trials.

Table 11. Selection of Experimental Data.

Parameter Type	Approach 1	Approach 2	Approach 3
Pressure (MPa)	3	5	7
Stirring Rate (RPM)	300	400	500

The experimental observations and analysis revealed that elevated pressure significantly accelerated acid etching and fracture propagation, thereby shortening experimental cycles. However, pressures exceeding 8 MPa posed a risk of inducing microfractures in the epoxy coating, leading to potential leakage. Controlled agitation was crucial for ensuring a homogeneous reaction interface and minimizing deviations between parallel samples, although sustained high speeds (>600 RPM) were found to induce vortices that lifted rock fines and trapped air bubbles. The optimization process involved systematically tuning the temperature, pressure, and catalyst dosage. Key principles included utilizing suitable temperatures to enhance the molecular motion and collision frequency, applying moderate pressure to stabilize the system while modulating solubility and diffusion rates, and implementing precision catalyst dosing to improve reaction kinetics and selectivity. In conclusion, based on a comprehensive balance of performance and operational safety, 5 MPa was identified and selected as the recommended operating condition.

4.4. On-Site Construction Materials

The formulas for the fluids used in the on-site construction process are as follows. The pre-pad fluid consisted of 450 kg of NH4Cl mixed with 15 m^3 of fresh water. Through indoor acid fluid reaction experiments, the optimized acid fluid formula was determined: 92.5 tons of 20% hydrochloric acid, supplemented with 2 tons of retarder SPR-12, 3 tons of a corrosion inhibitor, 1.5 tons of an iron stabilizer, and 1 ton of a displacement aid. The displacement fluid was composed of 31 m^3 of fresh water. The overall acid fracturing process is illustrated in Figure 11.

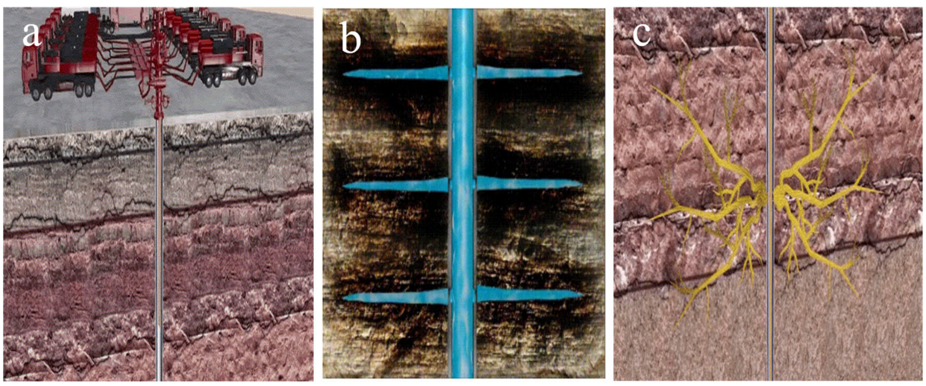

Figure 11. Acidizing and fracturing process diagram. (**a**) Pre fluid fracturing and cooling of the formation (Video S1); (**b**) Acid injection and etching of cracks; (**c**) Substitution and closure reaction.

4.5. Actual Monitoring Data of the Well After 6 Months

As shown in Table 12, after six months, the water inflow rate exhibited a mere 2.6–7.8% decline from the initial post-acid fracturing period (100.4 m^3/h), which is significantly lower than the industry average decay range of 15–20%. The decline pattern demonstrated that 'greater drawdown leads to slightly higher attenuation' (large drawdown: 7.8% decline; small drawdown: 2.6% decline), yet the overall reduction remained well-controlled, indicating sustained fracture conductivity integrity. The pumping influence radius systematically decreased with the reduced drawdown (ranging from 235 to 285 m), while stable continuation periods exceeded 60 h across all drawdown scenarios, confirming the long-term conductive stability of the acid-stimulated fracture pathways.

Table 12. The main monitoring parameters of this production well.

Item	Large Drop Rate	Medium Drop Rate	Small Drop Rate
Water Temperature (°C)	88.2	88.5	89
Inflow Rate (m^3/h)	92.6	95.3	97.8
Dynamic Water Level Burial Depth (m)	165.4	162.1	159.7
Duration (h)	72	72	72
Static Water Level Burial Depth (m)	248.3	248.5	248.2
Initial Fluid Level Temperature (°C)	88	88.3	88.8
Pumping Influence Radius (m)	285	260	235
Hydraulic Conductivity (m^2/d)	1862	1945	2018
Permeability (μm^2)	1.52×10^{-3}	1.61×10^{-3}	1.68×10^{-3}

The permeability consistently was maintained at 1.52×10^{-3}–1.68×10^{-3} μm^2, representing a 105–127% improvement over pre-acid fracturing values (peaking at 0.74×10^{-3} μm^2), validating the sustained effectiveness of the novel acid formulation. The water temperature remained above 88 °C throughout the experiment, with dynamic water level fluctuations below 6 m amplitude, reflecting stable reservoir energy replenishment and the absence of significant formation damage. The static water level stabilized at 248.2–248.5 m over the long term, demonstrating minimal deviations from pre-acid fracturing levels (250 m). Coupled with persistently high temperatures (>88 °C), these observations indicate a balanced reservoir energy supply without risks of prolonged formation impairment or depletion.

Hydraulic conductivity coefficients stabilized at 1862–2018 m^2/d across drawdown intervals, achieving orders-of-magnitude enhancements compared to the pre-treatment reservoir permeability (maximum 0.74×10^{-3} μm^2). This proves the sustained effective connectivity within the fracture network. The results demonstrate that the innovative acid system effectively mitigates fracture closure and secondary mineral precipitation, enabling production enhancements while reducing acid consumption—thereby demonstrating superior technical and economic advantages.

Supplementary Materials: The following supporting information can be downloaded at: https://www.mdpi.com/article/10.3390/pr14030563/s1, Videos S1 and S2: Acidizing and fracturing process diagram; Video S3: Schematic diagram of dynamic monitoring results of fractures in an experimental well.

Author Contributions: L.S. and F.L. conceived and designed the experiment and conveyed the manuscript information as corresponding authors. L.S. repeated the experiment multiple times and then used it as an in-depth research content. L.S. designed and wrote the manuscript. L.S. carried out the methodology, calculation, and writing the original draft preparation. F.L. finished the visualization, investigation work. All authors have read and agreed to the published version of the manuscript.

Funding: This research received no external funding.

Data Availability Statement: The original contributions presented in this study are included in the article/Supplementary Materials. Further inquiries can be directed to the corresponding author.

Conflicts of Interest: The authors declare no conflicts of interest.

References

1. Zhao, T.; Liu, Y.Q.; Zhang, J.B. Fracture identification and characterization of ultra-deep strike-slip fault-controlled carbonate reservoirs in Shunnan area, Tarim basin. *Carbonates Evaporites* **2025**, *40*, 95. [CrossRef]
2. Chen, Z.H.; Grasby, S.E.; Hedhli, M. Heat resource potential and reservoir characteristics of fractured and dolomitized carbonates of the Beaver River gas field, Liard Basin, western Canada. *Geotherm. Energy* **2025**, *13*, 30. [CrossRef]
3. Han, S.H.; Dawa, N.; Zhao, L.; Nima, G.; Bianma, C.C.; Zhao, H.H.; Zheng, Y.D.; Xiao, P. Hydrochemical characteristics and formation mechanism of geothermal fluids in Zuogong county, Southeastern Tibet. *Water* **2024**, *16*, 2852. [CrossRef]
4. Cui, Z.P.; Feng, B.; He, S.Q.; Liu, Z. Numerical modeling of the mechanical-chemical coupling effects of acid fracturing on carbonate geothermal reservoir: A case study of the Well D22 in Xiong'an New Area, China. *Geoenergy Sci. Eng.* **2026**, *257*, 214276. [CrossRef]
5. Wu, X.H.; Li, P.; Miao, S.J.; Cai, M.F.; Liu, Y.; Wang, M.; Xiong, W.S. Multi-field coupling mechanism and optimization of heat transfer in deep carbonate geothermal reservoirs based on acid fracturing modification. *Case Stud. Therm. Eng.* **2025**, *73*, 106591. [CrossRef]
6. Mao, D.Y.; Zhang, J.; Hoshino, Y.; Satake, S.; Yang, H.J.; Kuramitz, H.; Ueda, A.; Terai, A. Geochemical study of fluid origin and caprock formation with carbonate mineral precipitation in the Okuaizu geothermal area. *Geothermics* **2025**, *127*, 103242. [CrossRef]
7. Rehman, N.; Jiang, S.; Ali, H.S.; Ali, S.H.; Naz, A.F.; Tariq, M. Effect of diagenetic processes and depositional facies on reservoir quality of the eocene carbonate sequence (sakesar limestone) in the central salt range, Pakistan. *J. Earth Sci.* **2025**, *36*, 1129–1148. [CrossRef]
8. Li, Y.Y.; Zhang, E.; Yue, P.; Zhao, H.; Xie, Z.W.; Li, W. Simulating Water Invasion Dynamics in Fractured Gas Reservoirs. *Energies* **2024**, *17*, 6055. [CrossRef]
9. Moradi, M.; Kadkhodaie, A.; Kadkhodaie, R.; Saedi, G.; Wood, D.A. Depositional and diagenetic features of carbonate reservoirs determined from image logs and their impact on oil production. *Geoenergy Sci. Eng.* **2025**, *253*, 214002. [CrossRef]
10. Liu, J.; Zhang, W.Q.; Xue, Y.; Wang, H.M.; Li, S.T.; Zhang, Y.; Li, W.H. Evaluation of acid fracturing in carbonatite geothermal reservoirs based on a coupled thermo-hydro-mechanical-chemical model considering discrete fracture networks. *Geomech. Energy Environ.* **2025**, *43*, 100704. [CrossRef]
11. Jia, Y.C.; Li, L.; Wang, H.C.; Yang, M.; Liu, Q.; Li, J.S. Research on the mechanism and process of fracture reduction for high stress reservoirs. *J. Phys. Conf. Ser.* **2025**, *3048*, 012044. [CrossRef]
12. Zhu, Y.; Li, X.P.; Liao, L.; Feng, D.Q.; Mao, Y.K.; Li, J.Q.; Zhang, H. Experimental study of starting pressure gradient in carbonate gas reservoirs. *Geotech. Geol. Eng.* **2024**, *43*, 22. [CrossRef]
13. Zhang, Z.H.; Qi, N.; Zhou, S.M.; Zhao, G.Q.; Jiang, P.; Li, A.H.; Su, X.H. Numerical simulation and analysis of acid-etched surface morphology in carbonate reservoirs under stress. *Geoenergy Sci. Eng.* **2025**, *254*, 213997. [CrossRef]
14. Kong, X.W.; Shi, X.; Xie, G.Y. Numerical characterization of acid fracture wall etching morphology and experimental investigation on sensitivity factors in carbonate reservoirs. *Geoenergy Sci. Eng.* **2024**, *237*, 212762. [CrossRef]
15. Cao, X.S.; Ren, J.C.; Xin, S.Y.; Guan, C.C.; Zhao, B.; Xu, P.X. Study of acid fracturing strategy with integrated modeling in naturally fractured carbonate reservoirs. *Processes* **2024**, *12*, 808. [CrossRef]
16. Xu, H.R.; Cheng, J.R.; Zhao, Z.H.; Lin, T.Y.; Liu, G.H.; Chen, S.C. Coupled thermo-hydro-mechanical-chemical modeling on acid fracturing in carbonatite geothermal reservoirs containing a heterogeneous fracture. *Renew. Energy* **2021**, *172*, 145–157. [CrossRef]
17. Guo, A.B.; Tang, X.H.; Qiao, J.M.; Zhou, L.B.; Luo, P.D. Three-dimensional simulation of the acidizing process under different influencing factors in fractured carbonate reservoirs. *Energy Sci. Eng.* **2023**, *11*, 3102–3118. [CrossRef]
18. Aljawad, M.S.; Schwalbert, M.P.; Mahmoud, M.; Sultan, A. Impacts of natural fractures on acid fracture design: A modeling study. *Energy Rep.* **2020**, *6*, 1073–1082. [CrossRef]
19. Xu, J.Z.; Zhai, C.; Qin, L. Mechanism and application of pulse hydraulic fracturing in improving drainage of coalbed methane. *J. Nat. Gas. Sci. Eng.* **2017**, *40*, 79–90. [CrossRef]
20. Tian, J.; Kang, Y.L.; Luo, P.Y.; You, L.J.; Zhang, D.J. A new method of water phase trapping damage evaluation on tight oil reservoirs. *J. Pet. Sci. Eng.* **2019**, *172*, 32–39. [CrossRef]
21. Teixeira, B.J.; Silva, L.D.; Andrade, L.Â.; Fabris, J.D.; Fazio, G.; Candido, M.; Trindade, R.I.F. Interaction of the naphthalene-induced catalysis and leaching of magnetite: Insights on acid fracturing for oil and gas recovery efficiency. *J. Pet. Explor. Prod. Technol.* **2025**, *15*, 138. [CrossRef]

22. Zhao, H.F.; Liu, Z.Y.; Yu, C.J.; Gan, G.P. Study on the propagation law of acid fracturing in cave carbonate rock. *Environ. Earth Sci.* **2025**, *84*, 214. [CrossRef]
23. Liu, P.L.; Hu, H.T.; Chen, X.; Du, J.; Liu, J.M.; Liu, F.; Chen, W.H.; Jia, Y.C. The influencing parameters and improve methods of acid-etched fracture conductivity: A review. *Geoenergy Sci. Eng.* **2024**, *238*, 212844. [CrossRef]
24. Lin, Y.; Ke, B.; Yang, M.; Liu, Q.; Xiong, Q.; Niu, S.; Huang, L. Research and Application on the Mechanism of Carbonate Reservoir Acidizing Fracturing for Production Enhancement. *Urban Geol.* **2018**, *13*, 21–26. [CrossRef]
25. Du, J.; Li, J.L.; Liu, J.M.; Liu, J.M.; Liu, J.P.; Xiong, P.; Chen, P.F.; Li, Y.C.; Tian, W.H.; Zuo, Z.X. Evaluation of comprehensive acid fracturing performance of a new environmentally friendly acid for high-temperature carbonate reservoirs. *Geoenergy Sci. Eng.* **2025**, *254*, 214020. [CrossRef]
26. He, T.S.; Luo, Z.F.; Cheng, L.; Xie, Y.Z.; Zhao, L.Q.; Shang, L.; Jia, Y.C. Simulation study on acid fracturing productivity of fractured carbonate reservoir based on thermal-hydraulic-mechanical-chemical field couped. *Chem. Technol. Fuels Oils* **2025**, *61*, 511–523. [CrossRef]
27. Qiu, T.; Wei, Y.S.; Liu, P.C. Improved composite-productivity model considering acid fracturing in carbonate gas reservoirs. *Geoenergy Sci. Eng.* **2025**, *254*, 214047. [CrossRef]
28. Zeng, Q.D.; Li, T.X.; Bo, L.; Zhou, K.; Zhang, W.; Yao, J. Effect of acid pre-treatment on hydraulic fracturing in heterogeneous porous media. *Geoenergy Sci. Eng.* **2025**, *246*, 213601. [CrossRef]
29. Ren, J.C.; Liu, Z.L.; Deng, Y.; Guo, J.C.; Lai, J.; Wang, J.F.; He, S.G. The quantitative study of residual acid damage of low permeability carbonate rock based on NMR test. *Geoenergy Sci. Eng.* **2024**, *241*, 213109. [CrossRef]
30. Hu, J.; Yang, S.; Bi, L.; Gao, X.; Deng, H.; Zhao, E. Numerical modeling of CO_2 storage and gas recovery enhancement in low-permeability carbonate reservoirs via acid-fractured horizontal wells. *Fuel* **2026**, *404*, 136397. [CrossRef]
31. Xiong, D.; Zhang, L.F.; Xiao, C.; Wang, X.L.; He, J.Y. A novel post-fracturing evaluation method for fractured-vuggy carbonate reservoir by using pumping-stop pressure drop. *Geoenergy Sci. Eng.* **2025**, *254*, 214037. [CrossRef]
32. Zhang, Y.; An, G.F.; Mao, J.C.; Chen, A.; Wang, Q.H.; Qing, S.H.; Zhang, H.; Xiao, Y.K.; Mao, J.H.; Liu, W.; et al. A safe and environmental-friendly solid acid with sustained release, high etching, and low corrosion. *Geoenergy Sci. Eng.* **2024**, *237*, 212785. [CrossRef]
33. Nicolás, R.J.; Kong, X.Z.; Anna, K.; Luiz, G.M.; Ma, N.; Federico, G.; Maren, B.; Stefano, M.B.; Martin, O.S. Reactivity of wet scCO_2 toward reservoir and caprock formations under elevated pressure and temperature conditions: Implications for CCS and CO_2-Based geothermal energy extraction. *Energy Fuels* **2025**, *39*, 1679−1693. [CrossRef]
34. Li, C.; Yao, Y.; Pan, D. Unveiling hidden reaction kinetics of carbon dioxide in supercritical aqueous solutions. *Proc. Natl. Acad. Sci. USA* **2024**, *122*, e2406356121. [CrossRef]

https://doi.org/10.3390/pr14030563